Progress in Photovoltaics: Research and Applications

WILEY

PROGRESS IN PHOTOVOLTAICS

SPECIAL ISSUE ARTICLE OPEN ACCESS

Liquid PV Module Encapsulation to Enable Circular Design

Urvashi Bothra[1] | Sebastian Weemaes[1] | Thomas Rijsman[1] | Alberto Poli[2] | Siemen Brinksma[2] | Olindo Isabella[1] | Malte Ruben Vogt[1]

[1]Delft University of Technology, Photovoltaic Materials and Devices Group, Delft, the Netherlands | [2]Biosphere Solar, Rotterdam, the Netherlands

Correspondence: Urvashi Bothra (ubothra@tudelft.nl) | Malte Ruben Vogt (m.r.vogt@tudelft.nl)

Received: 5 September 2025 | **Revised:** 11 December 2025 | **Accepted:** 22 December 2025

Keywords: accelerated ageing | circular PV design | liquid encapsulation | PV module

ABSTRACT

The current industrial standard photovoltaic (PV) modules are dominated by crystalline-silicon (c-Si) PV technology, which cannot be easily recycled. This has generated worldwide concerns regarding the scarcity of critical raw materials and large waste streams of PV modules in the coming years. To overcome this problem, a lot of ongoing research focuses on upscaling the recycling process of present c-Si module designs by chemical, thermal and mechanical processes. Alternative research focuses on the development of new PV modules with enhanced circularity by design. In this work, we propose a new circular PV module design based on liquid-encapsulation technology in which silicon solar cells are encapsulated with a suitable liquid and an edge sealant instead of a polymer sheet. Our optical studies show that the selected liquids exhibit similar optical performance to ethylene vinyl acetate (EVA) due to their comparable refractive indices. We fabricate one-cell prototypes and observe comparable efficiency of liquid-encapsulated and EVA-encapsulated modules, signifying recyclable module design without an additional efficiency loss. To validate the module performance, we also simulate the optical performance of modules with different encapsulation materials. Furthermore, the new modules retained more than 95% of their efficiency after inducing accelerated ageing through damp heat, thermal cycling and humidity freeze tests, indicating the liquids as an excellent encapsulant material for PV. In the end, we disassemble the liquid-filled PV module and show the recovered components, which can directly be reused in new products. Therefore, this modular design bypasses the recycling process. Even more promising, the liquid encapsulation can improve the stability of perovskite/c-Si tandem solar cells due to the moisture barrier, which will be studied in the future. Adding further possibilities, in principle, with additional engineering, the liquid encapsulation could be used in a heat loop to turn the PV module into a photovoltaic-thermal (PV-T) module, thereby boosting the efficiency potential beyond that of traditional PV concept.

1 | Introduction

The photovoltaic (PV) module deployment has grown rapidly in the last few years to adhere to the Paris climate agreement by trying to ensure the global increase in temperature remains below 1.5°C [1, 2]. The worldwide installations have increased from 1 TW to 2 TW in the last 2 years, highlighting the exponential growth in installations and consequently, the module production [3]. Moreover, PV installations are projected to increase further due to it being one of the cheapest forms of electricity generation when looking at the levelized cost of electricity [4]. However, the increased solar panel installations are estimated to generate a waste stream of 212 million tonnes from PV modules reaching their end-of-life (EoL) by 2050 [5]. Furthermore, with the increased PV deployment, the annual indium and silver demand may exceed their global mining production before 2040 [6]. This has generated worldwide concerns and a need for designing circular PV modules, which can be repaired to extend the module's lifetime, reused and eventually recycled to use the critical materials multiple times in a circular economy.

One of the biggest limiting factors toward high quality recycling of the existing solar panel is ethylene vinyl acetate (EVA) lamination, which makes it difficult to separate the module components. Moreover, degradation of EVA is a serious problem; therefore, research is going on to design new encapsulants such as cleavable epoxy resins [7], nanostructured polymer [8] and bio-based polymer encapsulants [9]. At present, after removing the aluminium frame and junction box, most of the PV panels at the EoL result either in landfills or are downcycled by mechanical shredding [10, 11]. A lot of cumulative research and development effort has been done to separate the PV components, for efficient recovery of important PV materials such as silicon (Si), silver, etc. This can be achieved by (i) finding new cost-effective technical solutions to separate components of the existing PV modules and (ii) designing new PV modules, which can enable easy disassembly. Some of the high-value recycling processes include various mechanical, chemical, thermal processes and even their combination to recover high purity materials [12]. Other complex delamination processes adopted by Flaxres, NPC and LuxChemtech include short light pulses, hot knife and water jet methods, which can result in the reuse of solar glass [13–15]. Although these technological advancements are important for upcycling of PV materials, at present they are cost- and energy-intensive, making these processes less attractive for industrial application [16].

The alternate route for efficient recycling involves 'Design for circularity,' which aims at designing PV modules that can be easily separated into their components [17, 18]. This also allows easier reuse and repairs, making them suitable for the circular economy. In 2004, Apollon Solar introduced one such PV module design called the new industrial solar cell encapsulation (NICE) [19]. In the NICE module design, the encapsulant is replaced by inert air and an edge sealant; additionally, the modules are solder-free and electrical connection is made by forcing copper ribbon and cell-busbar to contact via underpressure between front and back glass [20]. NICE modules passed IEC tests and showed excellent stability under accelerated ageing with $<2\%$ power degradation [21]. Another module design called TPedge was proposed by Fraunhofer ISE, which used air encapsulation and double edge sealant [22]. Although these designs show easy disassembly of modules, they lack in the aspect of module efficiency compared to conventional modules [23, 24]. This is due to increased reflection losses in these modules because of suboptimal refractive index matching at the internal glass–air interface. To mitigate the reflection losses in these designs, a new design was conceptualized by the cooperation of Biosphere Solar and TU Delft in which air is replaced by a liquid of optimal refractive index [25, 26]. Recently, another design built on the NICE modules was proposed by Perelman et al., where a combination of a polymer layer and a liquid layer is used as an encapsulant [27].

In this work, we design novel liquid-filled circular PV modules, which can be repaired, repurposed and recycled because of the ease of disassembly of the module. Firstly, we select eight appropriate liquids by studying their various optical, electrical, physical, chemical and thermal properties. Afterwards, we perform a detailed comparison of air-, liquid- and EVA-encapsulated c-Si PV modules by studying their optical, electrical and reliability behaviour. We simulate PV modules with different encapsulation to validate and analyse the experimental results. Finally, we demonstrate the disassembly of the liquid-filled PV module into individual components, such that each component can be accessed on a modular level resulting in a higher level of circularity.

2 | Methods

2.1 | Materials and Module Fabrication

The front and back glass used in this study are 25 cm × 25 cm and 4-mm thick tempered, nonsolar float glass without antireflection coating from Balink Glas & Aluminium. The 50 cm × 50 cm glass with four circular openings is purchased from AGC glass. The liquids used in the study are silicone oil (XIAMETER PMX-561 from DOW chemicals), hydrocarbon-E (Electrocool EC-110 from Engineering fluids), ester oil (MIVOLT DFK from MIDEL & MIVOLT Fluids), hydrocarbon-O (Opticool-H from DSI Ventures), SP glycol (SolarPro from InnogreenChem), glycol (Monopropylene glycol from Labshop), glycerol (Glycerine 99.5% from Labshop) and DI (deionized) water. Polyisobutylene (PIB, HelioSeal pvs 101 from Kömmerling-H.B. Fuller) is used as the edge sealant. Commercially available EVA is used as an encapsulant for manufacturing the commercial module. 12.5 cm × 12.5 cm Maxeon Gen III Interdigitated back contact (IBC) solar cells from SunPower Corporation are used here. For the electrical connections, dogbone connectors and busbars are ordered from Qinhuangdao Donwoo Electronic and Ulbrich, respectively.

The schematic of the cross-section of the liquid-filled module is shown in Figure 1a. To manufacture one-cell module prototypes, IBC cells are soldered with dog bones and busbars as shown in Figure 1b. Afterwards, the PIB edge sealant is placed on the edge of the bottom glass, and the soldered Si cell is laminated between the two glass sheets using an Experia PV laminator to complete the structure as shown in Figure 1c. The lamination is carried out at 95°C and 400-mbar pressure to enable complete sealing of the module without inducing cracks in the cell. This completes the air-filled modules. Liquid-filled modules are manufactured by filling liquids in the air-filled modules through PIB using a syringe as shown in Figure 1d. Simultaneously, another needle is used to create a small gap through PIB to extract air from the module. The final step involves removing the needle and syringe to reseal the PIB using a heat gun. For the EVA reference modules, the EVA sheet is placed below and above the soldered cell with interconnects, followed by the top and bottom glasses. In contrast to the liquid-filled modules, due to the higher melting point of EVA than PIB, EVA lamination is done at 150°C at 900 mbar. The lamination conditions for the air-filled, liquid-filled and EVA encapsulated modules are shown in detail in Table S1.

The optical studies and the liquid-PIB compatibility studies are carried out by making a glass/encapsulant+PIB/glass sandwich structure for air and liquid encapsulation and glass/EVA/glass for EVA encapsulation. The samples are laminated with the same processing conditions as the modules, as shown in Table S1. Nonsolar float glass without antireflection coating of 5 cm × 5 cm area and 4-mm thickness is used for these studies.

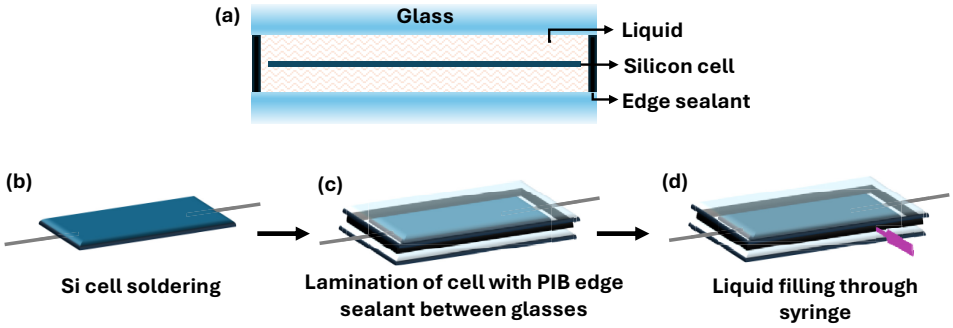

FIGURE 1 | Schematic of the (a) cross-section of liquid-filled module and (b–d) main steps of the process for manufacturing one-cell liquid-filled modules.

2.2 | Characterization

Light transmission (reflectance) is measured with a Perkin Elmer Lambda 1050 by placing the sample at the transmission (reflectance) port of the integrating sphere. The current–voltage (I–V) measurements are performed by illuminating the PV module using an Enlitech solar simulator and measuring the modules using a Keithley 2651A source meter. The solar simulator is calibrated using a reference cell. The modules are measured at the standard testing conditions of 1000 W/m^2 incident solar radiation, 25°C cell temperature and Air Mass 1.5 spectrum [28]. Electroluminescence (EL) imaging of the modules is carried out by applying 0.7 V using an EA-PS 9200-25 power supply from Elektro-Automatik. The EL image is captured by a Nikon AF-S NIKKOR camera.

2.3 | Reliability Tests

The accelerated ageing tests on the modules are performed using ESPEC PL-3J climate chamber following the IEC-61215 norm [29]. Damp heat (DH) test is performed by keeping the modules in climate chambers at 85°C and 85% relative humidity. Thermal cycling is performed by varying the chamber temperature from −40°C to 85°C such that one complete cycle takes 6 h. Another test carried out is the humidity freeze test, which takes 24 h to complete a cycle. In each humidity freeze cycle, the modules are kept at 85°C and 85% RH for 20 h followed by 4 h of thermal shock where the temperature is decreased from 85°C to −40°C and increased back to 25°C.

2.4 | Optical Simulations

The optical simulation of the module stack is performed by GenPro4 [30] software using as input the thickness and the wavelength dependent (300–1200 nm) refractive index (n) and extinction coefficient (k) of the materials involved. The n values of silicone oil, ester oil and glycerol are measured using a Semilab SE-2000 ellipsometer and the k values are obtained through the dual cuvette method using a Perkin Elmer Lambda 1050 spectrometer [31]. The complex refractive index for all the other layers is taken from the Genpro4 database. The IBC cell layer configuration used for simulation is adopted from Lizcano et al.'s work [32].

3 | Results and Discussion

3.1 | Liquid Encapsulant Properties

It is important to choose an appropriate liquid, which can be used as an encapsulant. Some of the properties, which are important and considered while choosing a liquid encapsulant are toxic, thermal, physical, chemical, optical, and electrical properties [33]. Table 1 summarises the properties of the eight selected liquids compared to the EVA. After a comprehensive search, we selected liquids from different classes, such that we included two oils (silicone oil and ester oil), two synthetic hydrocarbons (hydrocarbon-E and hydrocarbon-O), two glycols (SP glycol and glycol), glycerol and DI water. An important criterion for the sustainability of the circular PV modules is the nontoxicity of the liquids; therefore, all the chosen liquids are ensured as nontoxic in nature.

In the outdoor conditions, the temperature of PV modules ranges from −40°C to 85°C. To ensure outdoor temperature conditions align with the working temperature range of the liquids, all selected liquids have flash point >100°C and pour point <−40°C, except glycerol (pour point 18°C) and DI water (freezing point 0°C). Alcohols such as isopropyl alcohol and ethanol are not included because of their low boiling points and low flash points. We also compared the thermal conductivity of all the liquids as shown in Table S2. The thermal conductivity of encapsulants should be high to facilitate heat dissipation from the silicon cell. Table S2 shows that most of the studied liquids have thermal conductivity ranging from 0.147–0.187 W/(m·K), which is slightly lower than EVA (0.23 W/(m·K)), except for glycerol (0.292 W/(m·K)) and DI water (0.624 W/(m·K)). To improve the thermal conductivity, liquids can be blended with glycerol and DI water. Other important thermal properties of the liquid include high heat capacity and low thermal expansion.

Furthermore, the injected liquid should not increase the weight of the module compared to EVA. Therefore, the weight of the liquid in a one-cell module is calculated from its density and volume (~40 mL of liquid) used. In a one-cell module, the weight of all liquids (except SP glycol) is lesser than the weight of EVA sheets as shown in Table 1. For the same module (with ~40 mL of liquid encapsulation), the approximate cost of encapsulant used is 0.03 € for DI water [49], 0.1 € for EVA [50] and 0.1 € for silicone oil [51].

TABLE 1 | Properties of the selected liquids used in this work. The selected liquids have properties comparable to EVA. The weight of a one-cell module is calculated from the volume and density of liquid (or EVA) used.

Liquid	Flash point (°C)	Weight in one-cell modules (g)	Electrical resistivity (Ωcm)	Refractive index
Silicone oil	> 300 [34]	~40 [34]	1×10^{14} [34]	~1.40–1.47 [31]
Ester oil	> 250 [35]	~40 [35]	$> 9\times10^{12}$ [35]	1.45–1.5 [31]
Hydrocarbon-E	203 [36]	~33 [36]	$> 1\times10^{14}$ [36]	~1.44 [36]
Hydrocarbon-O	135 [37]	~33 [37]	—	—
SP glycol	> 160 [38]*	~56 [38]	—	1.39–1.43 [38]
Glycol	103 [39]	~41 [39]	2×10^{7} [40]	~1.43 [39]
Glycerol	198 [41]	~50 [41]	$> 2\times10^{6}$ [42]	1.46–1.52 [31]
DI water	100*	~40	2×10^{7} [43]	1.33 [44]
EVA	90–120 [45]**	~51 [46]	1×10^{15} [47]	1.48–1.55 [48]

* and ** represent boiling point and melting point, respectively.

Moving forward to the electrical property, it is essential for the liquid encapsulant to be electrically insulant to prevent short-circuit, degradation and ensure safety. Therefore, the electrical resistivity of liquids is shown in Table 1. The electrical resistivity of silicone oil and hydrocarbon-E is comparable to EVA; however, it is lesser for other liquids. Moreover, the breakdown voltage values of the liquids are considered, which are mostly in the range of 20–30 kV/mm and comparable to the 30 kV/mm of EVA.

The optical properties of the encapsulant play a crucial role as it directly affects the device's performance. Therefore, the refractive index of the liquids should be similar to that of glass ($n \sim 1.5$) to avoid additional reflection losses as shown in Figure 2a. Table 1 shows the refractive index of the liquids in the range of 1.3–1.5, in contrast to that of air ($n = 1$). We further performed reflection and transmission experiments of glass/encapsulant/glass sandwich structure as described in Section 2.1. Figure 2b shows the reflectance spectra of the sandwich structure with reflectance of ~13% for the air-encapsulated glasses. Compared to air, a 4% decrease in reflectance is observed for DI water encapsulated samples. Moreover, the reflectance value is 6%–8% for other liquid- and EVA-encapsulated samples. This can be explained by the improved optical matching at the glass–encapsulant interface as shown in Figure 2a. Among the studied liquids, DI water shows highest reflectance due to $n \sim 1.33$ whereas hydrocarbon-O shows the least reflectance, which can be considered a liquid with high potential. Subsequently, Figure 2c shows transmittance spectra of these sandwich structures with 5%–6% less transmittance of air-filled compared to most liquids and EVA. The average transmittance in the range of 400–1100 nm of all the encapsulants in sandwich structure is shown in Table S3. Hydrocarbon-O shows least average transmittance of ~76%, which could be due to higher absorption of light in hydrocarbon-O. Among all studied encapsulants, EVA shows the highest average transmission (85.9%) closely followed by ester oil (85.34%) and silicone oil (85.17%). To summarize, most of the selected liquids show desirable properties, which are also comparable to EVA; therefore, they will be used for further experiments.

The module structure in Figure 1a shows that the edge sealant holds the liquid inside the structure and any damage to the edge sealant would lead to liquid leakage from the module. Therefore, it is important to examine the compatibility of liquids and the PIB edge sealant. Figure S1a shows the small glass/liquid/glass sandwich structures with silicone oil, hydrocarbon-E, ester oil and hydrocarbon-O liquids. To study the liquid-PIB interaction, the prototypes are kept in an ambient atmosphere in the dark for 4 months. Figure S1b shows all prototypes with a highlighted image of hydrocarbon-O, indicating its interaction with the PIB. Because of this, the sample with hydrocarbon-O is removed and will not be used in subsequent experiments. Furthermore, the remaining prototypes are kept in the climate chamber to study the effect of extreme conditions on their compatibility. Figure S1c shows the prototype images after 300 h of damp heat (85°C and 85% RH) test, which triggered the interaction between PIB and hydrocarbon-E. Therefore, although the synthetic hydrocarbons showed promising properties, they will not be used in the module manufacturing due to their interaction with PIB. However, hydrocarbons can be researched further with a compatible sealant in future work. We further added SP glycol and glycerol liquid samples and performed 51 thermal cycles (described in Section 2.2) in the climate chamber on them. Figure S1d finally shows the prototypes of silicone oil, ester oil, SP glycol and glycerol, which are intact through all the thermal cycle tests and will be used in module manufacturing. Because of the known water resistant property of PIB [52], DI water will also be used for the module encapsulation.

3.2 | Module Performance

Table 2 shows the average performance parameters of one-cell modules with EVA, air and liquid encapsulations. Because of measurement of only one module, the performance parameter of SP glycol module is not shown here. For comparison, the performance parameters of bare IBC cells is also mentioned from its data sheet [53]. The EVA encapsulated module shows efficiency of 22.6%, with 1.6 mA/cm^2 decrease in short circuit current density (J_{SC}) and ~2% decrease in fill factor (FF) compared to the

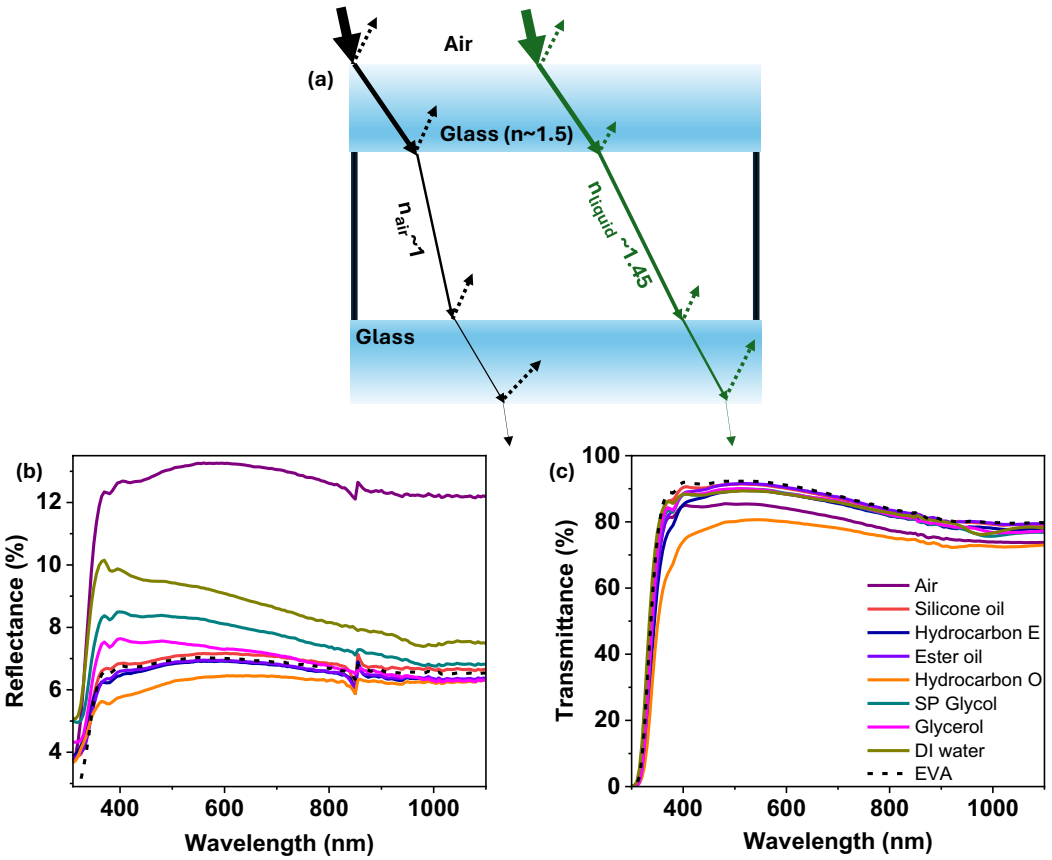

FIGURE 2 | (a) Schematic of optical ray passing through the different refractive index in glass–air (or liquid)–glass architecture. (b) Total reflectance and (c) transmittance for air, liquids and EVA (dashed line) sandwiched between glasses. The reflectance for glass–air–glass sample is 6% higher compared to liquid or EVA, due to suboptimal refractive index at the glass–air interface.

TABLE 2 | Performance parameters of the one-cell c-Si module encapsulated with air, liquids and EVA. The values represent average and standard deviation of at least three modules. Cell area of 155 cm^2 is used to calculate J_{SC} of the modules. Silicone oil–filled and EVA-encapsulated modules show the highest power conversion efficiency (PCE) of 22.6%.

	J_{SC} (mA/cm^2)	V_{OC} (V)	FF (%)	PCE (%)	CTM power ratio
Bare cell [53]	41.4 ± 0.1	0.732 ± 0.003	80.3 ± 0.2	> 24.4	
EVA	39.8 ± 0.9	0.733 ± 0.004	77.7 ± 0.4	22.6 ± 0.5	0.926
Air	38.0 ± 0.5	0.724 ± 0.006	77.7 ± 0.6	21.4 ± 0.4	0.877
Silicone oil	39.8 ± 0.1	0.728 ± 0.001	78.0 ± 0.2	22.6 ± 0.1	0.926
Glycol	39.5 ± 0.3	0.728 ± 0.002	77.9 ± 0.3	22.4 ± 0.6	0.918
Glycerol	38.7 ± 0.9	0.735 ± 0.005	77.4 ± 0.8	22 ± 0.6	0.902
DI water	38.9 ± 0.8	0.735 ± 0.003	78.1 ± 0.5	22.3 ± 0.4	0.914
Ester oil	39.1 ± 1.3	0.722 ± 0.004	77.4 ± 0.8	21.9 ± 0.6	0.898

bare cells. The cell to module (CTM) power ratio is 0.926 and the power losses are due to optical and electrical losses [54]. In contrast to the EVA case, the efficiency of air-filled modules is 21.4%, resulting in CTM_{air} power ratio of 0.877. This is due to higher optical losses in air-filled modules, as shown in Figure 2, leading to ~3 mA/cm^2 reduction in J_{SC}. Liquid-filled modules show efficiency higher than that of the air-filled modules. The efficiency of liquid-filled modules ranges from 21.9% to 22.6% with CTM_{liquid} power ratio of 0.898–0.926. Among the liquids, silicone oil showed the highest performance of 22.6%, which is also comparable to the EVA encapsulated module. Moreover, it is interesting to note that the range of efficiency for liquid-filled modules could be either due to different optical properties of the liquids or due to the varying initial performance of modules before filling the liquids. As these are hand-manufactured one-cell modules, manufacturing variability—especially related to soldering—could be present, which will be discussed in detail.

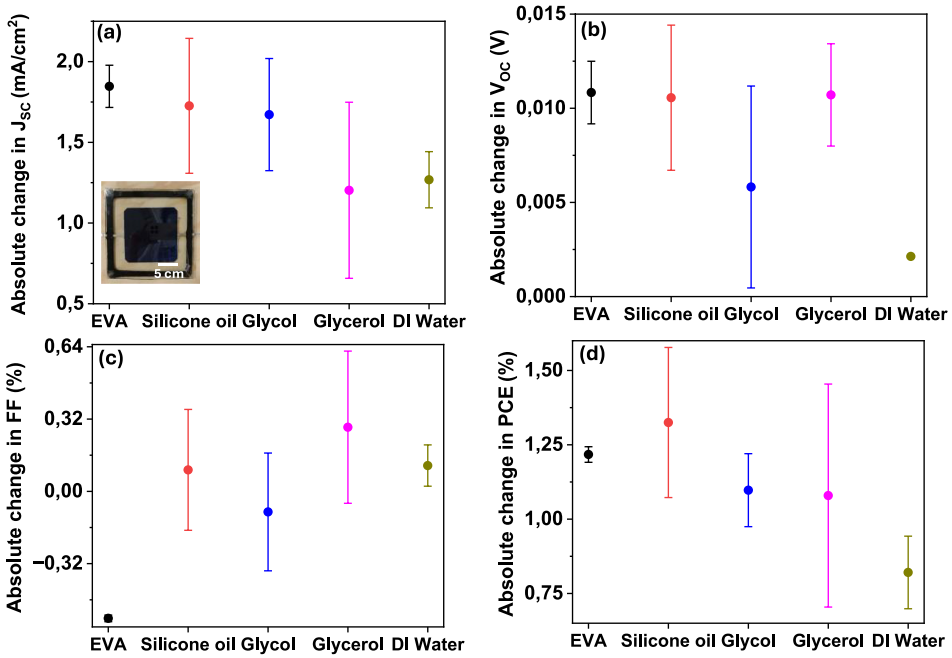

FIGURE 3 | Absolute change in (a) short circuit current density (J_{SC}), (b) open circuit voltage (V_{OC}), (c) fill factor (FF) and (d) power conversion efficiency (PCE) after filling liquids (or adding EVA) in air-filled modules. Inset image in (a) depicts one of liquid encapsulated one-cell mini module. All plots show mean and standard deviation of three modules for each encapsulant. Silicone oil–filled module shows the highest average improvement in PCE of 1.3%.

As described in Figure 1, before filling liquid in the modules, all the modules are air-filled. Thus, any variation in the performance of air-filled modules would affect the liquid-filled modules' performance as well. To accurately understand the effect of liquid filling on the efficiency of modules, the modules are measured before and after injecting the liquid. Figure 3a inset shows the image of a one-cell liquid-filled module. Figure 3a–d shows the average and standard deviation of the absolute change in module performance parameters after filling liquid in air-filled modules. It is important to note that the error bars in Figure 3 are different from the error bars in Table 2 due to initial variability in the performance of air-filled modules. To be consistent, we also measured the performance of EVA encapsulated modules before lamination, by placing glass below and above the soldered Si cell.

Liquid-filling or EVA-lamination in the air-filled module changes J_{SC} the most, with at least 1 mA/cm^2 increase in J_{SC} for all the encapsulants. This can be explained by gain in optical transmission due to better matching of the refractive index of glass with liquids and EVA. Among the studied encapsulants, EVA shows the maximum change in J_{SC} of 1.84 mA/cm^2. Silicone oil and glycol closely follow the trend with improvement of 1.75 mA/cm^2 and 1.67 mA/cm^2 while the lowest improvement is observed by glycerol with 1.25 mA/cm^2. Open circuit voltage (V_{OC}) of all the modules increased by 0–10 mV on adding liquid or EVA into the modules. The improvement in V_{OC} can be attributed to the reduced recombination losses as observed in the previous studies on the effect of dielectric liquid on silicon solar cells [55–57]. The absolute change in the FF of the modules shows a slight reduction after laminating (−0.56%) for the EVA reference, while filling liquid leads to ± 0.3% absolute FF change. Finally, Figure 3d shows the absolute change in PCE, which is highest for the silicone oil, followed by EVA, glycol, glycerol and DI water. These results slightly deviate from the efficiencies shown in Table 2, as glycerol outperforms DI water in Figure 3. This also explains the need to observe the absolute change upon liquid filling rather than the final efficiency to minimize error propagation due to manufacturing variation.

To validate the experimental results, we further performed simulations on the modules with air, silicone oil and EVA. Figure 4a shows the optical stack used in the simulation. Figure 4b–d shows the simulated absorbance spectra for EVA, air and silicone oil–filled modules, and the corresponding implied photocurrent density absorbed by each layer. The reflected irradiance from the module stack is highest for air-filled modules due to its low refractive index ($n = 1$), resulting in a current loss of 5.8 mA/cm^2. This led to 38.6 mA/cm^2 current density from the air-filled module. In contrast, due to better matching of the refractive index of EVA and the silicone oil with glass, the reflected light is reduced and the current density from EVA and silicone oil-filled modules is 40.2 mA/cm^2. Moreover, the simulation results are in the range of experimental values as shown in Table S4.

3.3 | Accelerated Ageing Tests

The liquid-filled modules are further subjected to accelerated ageing tests according to IEC 61215 to evaluate their performance under extreme conditions. Figure 5 shows the performance of EVA, air- and four liquid-filled modules under humidity freeze conditions. The humidity freeze test is performed to determine the module's ability to withstand penetration of humidity at extreme temperatures. For the modules to qualify, the power degradation should be < 5% at 10 humidity freeze

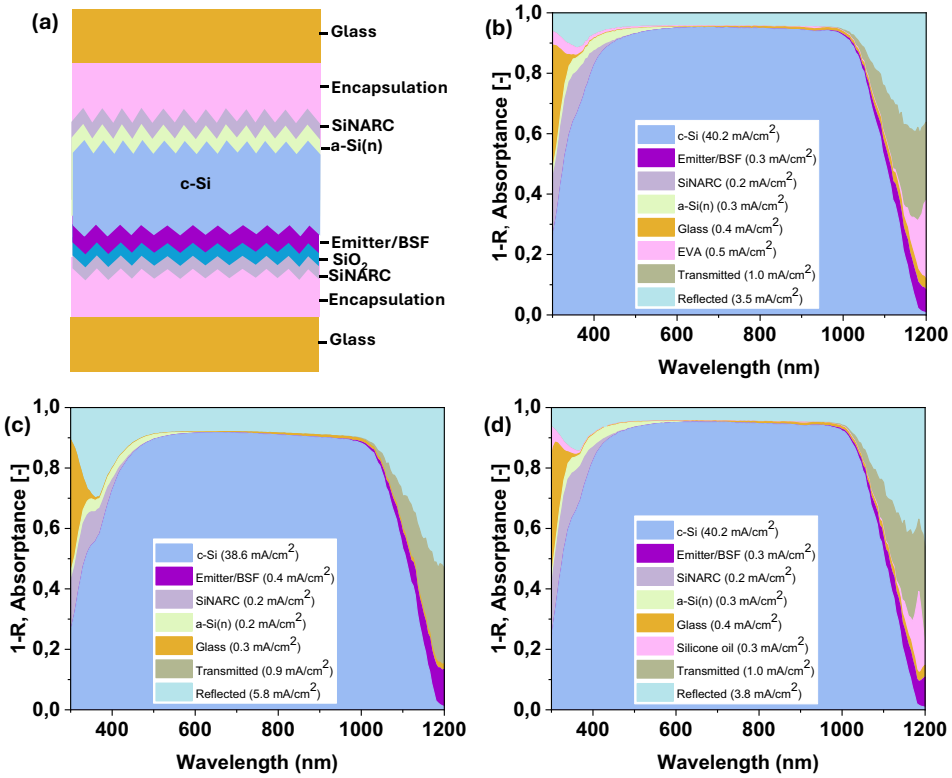

FIGURE 4 | (a) Schematic of cross-section of c-Si photovoltaic module. Simulated absorptance spectra of each layer of the module and its corresponding photocurrent for (b) EVA encapsulated, (c) air-filled and (d) silicone oil–filled module. Compared to air-filled modules, silicone oil–filled and EVA-encapsulated module show an increase of 1.6 mA/cm^2 in the implied photocurrent density of c-Si absorber.

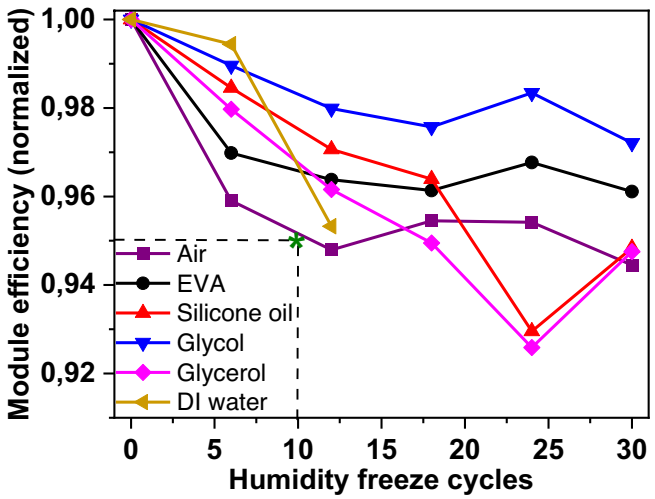

FIGURE 5 | Normalized module efficiency of air-filled, EVA-encapsulated, and liquid-filled modules as a function of humidity freeze cycles. Glycol-filled module shows the least degradation of 3% at 30 humidity freeze cycles while modules filled with DI water interact with Si cell and show early degradation. The dashed line shows threshold normalized efficiency of 0.95 at 10 humidity freeze cycle, required to pass the test. One sample of each encapsulant is tested here.

cycles [58]. At 10 humidity freeze cycles, all the modules show less than 5% of degradation, thus passing the test. However, after 12 humidity freeze cycles, DI water shows corrosion of busbars and interaction with Si cell, as can be observed in the EL images in Figure 6. Thus, the DI-water–filled module is not tested any further. Other modules are further evaluated in up to 30 humidity freeze cycles. Glycol-filled module shows the least degradation of 3% at 30 humidity-freeze cycles, while the air-, silicone oil- and glycerol-filled modules show degradation of ~5%. The degradation of air-filled module can also be observed in the EL images in Figure 6 where cracks are induced after 30 cycles, which can be due to the high thermal expansion of air. The degradation of air-filled modules observed here is higher than reported for NICE modules [20], probably due to the use of under-pressure in NICE modules. Figure 6 also shows EL images of EVA, silicone oil, glycol and glycerol modules, where no visual degradation after 30 humidity freeze cycles is observed. Figure S2 shows the evolution of J_{SC}, V_{OC} and FF as a function of 30 humidity freeze cycles. After an initial 2%–4% decrease in J_{SC} at five humidity freeze cycles, the J_{SC} is stabilized with final decrease of 2%–5% at 30 humidity freeze cycles. V_{OC} of all the modules is least affected by the humidity freeze cycles. The FF of all the modules is stable for 30 humidity freeze cycles except for ~2% decrease in case of silicone oil and glycerol.

Previous studies have shown that the single-stress nature of IEC 61215 tests is not enough to discover many failure modes; therefore, sequential stress tests can be important to further evaluate the module's resistance to degradation [59]. Thus, we performed a series of stress tests, which comprise 1300 h of damp heat followed by 200 thermal cycles and 10 humidity freeze cycles on the same modules. Therefore, the air- and three liquid-filled (silicone oil, SP glycol and ester oil) modules are tested for 4 months continuously under different stress conditions. Figure 7 shows the relative change in J_{SC}, V_{OC}, FF and PCE as a function of damp

heat time, thermal cycle and humidity freeze cycles. Damp heat test is performed to check the module's ability to withstand long-term penetration of humidity. Under 1300 h of damp heat test, air-filled module shows the most stability while the module filled with SP glycol shows > 10% degradation. Modules with silicone oil and ester oil show ~5% relative degradation due to ~5% decrease in J_{SC} and 1%–2% decrease in V_{OC} of modules. Moreover, for a module to pass damp heat test, its power degradation should be < 5% at 1000 damp heat hours [58], which is clearly not the case for SP glycol filled module. Visual inspection and EL imaging (Figure 8) of the SP-glycol-filled module show low light emission, cell degradation and corrosion of the

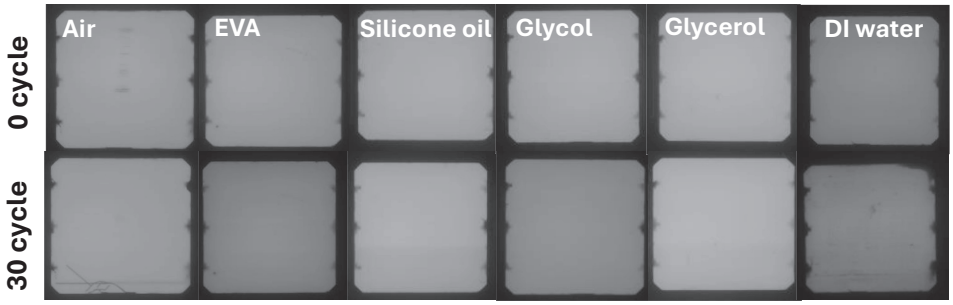

FIGURE 6 | EL images of the modules before and after 30 humidity freeze cycles (12 humidity freeze cycles for DI-water–filled module). The air-filled module shows induced cracks and DI-water–filled module shows interaction with c-Si cell, after humidity freeze cycles.

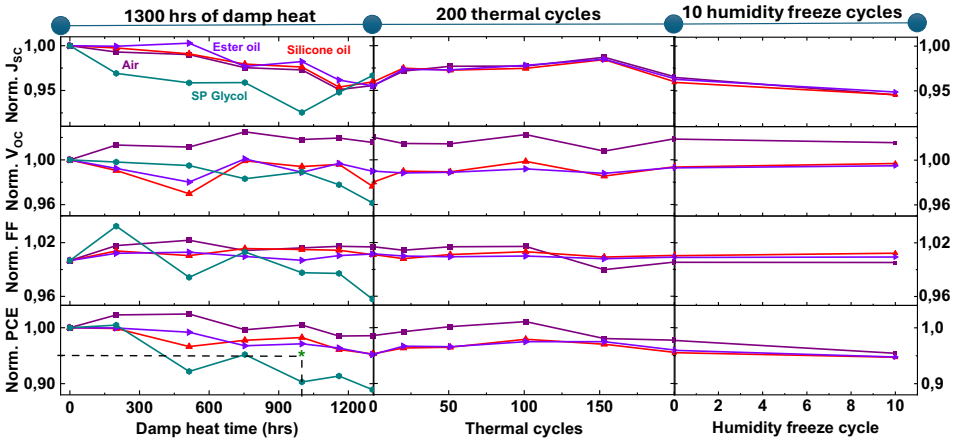

FIGURE 7 | Relay of accelerated ageing tests on the air- and liquid-filled modules: 1300 h of damp heat test followed by 200 thermal cycles, and 10 humidity freeze cycles. The cumulative test time is ~4 months. SP glycol filled module fails as the PCE decreases by more than 5% at 1000 h of damp heat. The dashed line at 0.95 PCE and 1000 damp heat hours represents the criterion to pass the test. One sample of each encapsulant is tested here.

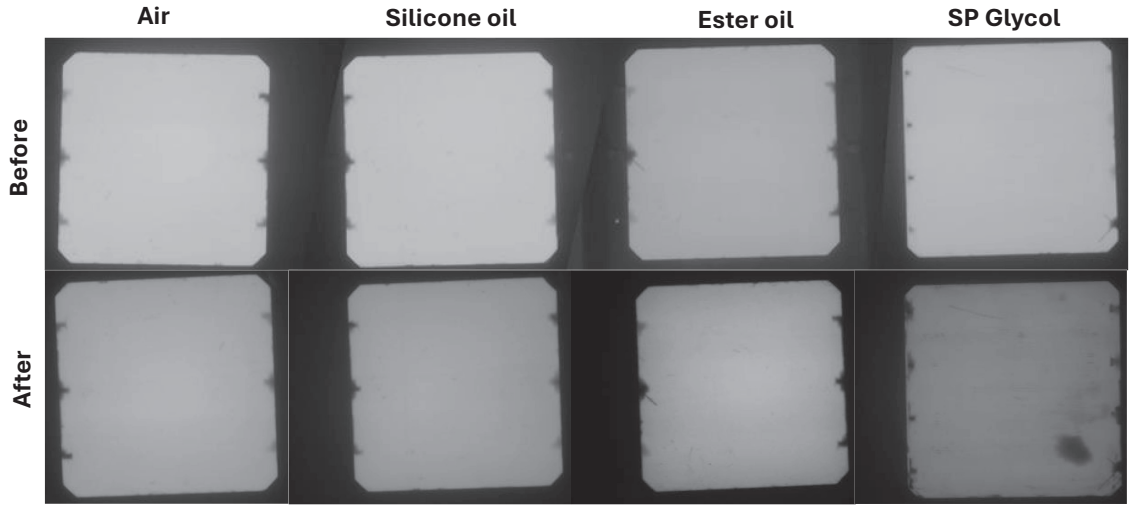

FIGURE 8 | Electroluminescence images of air- and liquid-filled modules before and after sequential accelerated ageing test (1300 h damp heat +200 thermal cycles +10 humidity freeze cycles). For SP glycol, the 'after' image is after 1300 damp heat hours due to its early degradation.

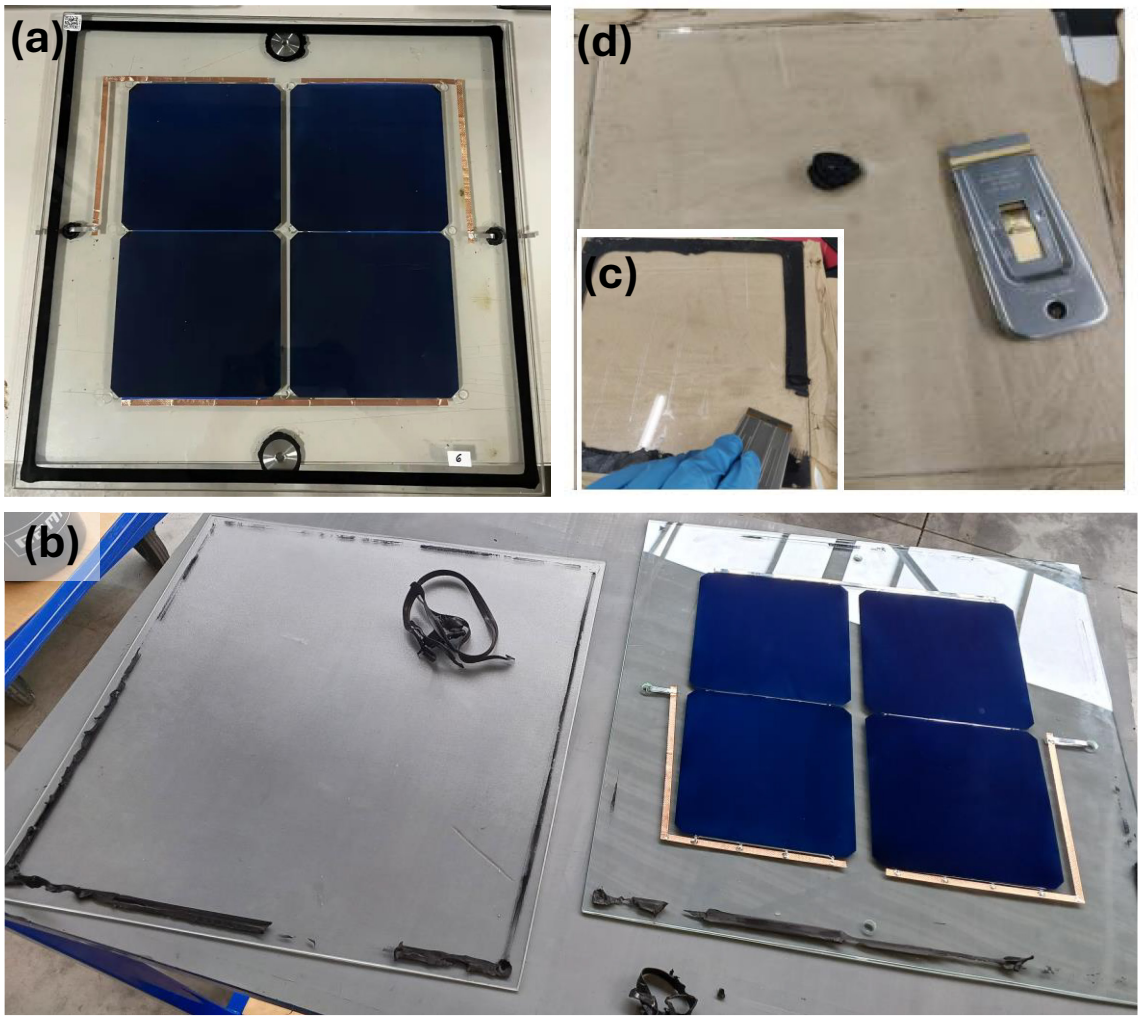

FIGURE 9 | Dismantling the liquid-filled module. (a) Sealed module, (b) liquid removal followed by module opening by cutting the PIB from the edges, (c) scraping of PIB and (d) removed PIB and cleaned glass. All the separated components can be either reused or recycled separately.

soldered contacts after 1300 h of damp heat. This could be due to the presence of water and other additives in SP glycol, which interacted with the solar cell. Therefore, we eliminate SP glycol from further tests.

Furthermore, we continue with 200 thermal cycles with the remaining modules: air, silicone oil and ester oil. Thermal cycling test is performed to simulate the effect of thermal stress on material's durability and 200 thermal cycles corresponds to module's performance in 10 years of outdoor exposure [60]. As shown in Figure 7, the performance of all the modules remains stable throughout the 200 thermal cycles with $<1\%$ decrease in relative efficiency of the modules, indicating excellent stability of all the modules under thermal stress. This is also in alignment with previous studies on NICE [19], TPedge [22] and the innovative concept [27] module where $<3\%$ of degradation was observed under 200 thermal cycles. Finally, we concluded the tests with 10 humidity freeze cycles on the same modules. The liquid-filled modules show a further 1% power degradation while air-filled module showed 2% power degradation. These results are also consistent with Figure 5, where comparatively larger degradation is observed in air-filled modules. The driver for degradation in all the modules is ~1% reduction in J_{SC}, while V_{OC} and FF remain unaffected. Figure 8 shows the EL images of air- and liquid-filled modules before and after the test. The module appears intact after the test and no new hotspot, crack, is observed in the air-, silicone oil- and ester oil-filled module. Therefore, these modules show excellent performance with only 5% degradation under the combined stress test of ~4 months. Table S5 shows an overview of which encapsulant passed (or failed) in each test performed in this work.

3.4 | Reusing and Recycling

The liquid-filled modules show great potential in terms of performance and reliability. In this section, we explore the circularity of these modules. Figure 9a shows a four-cell glycol-filled module, which is manufactured on 50 cm × 50 cm glasses with resealable openings for the liquid filling process. The device performance parameters of this module before and after glycol filling are shown in Table S6. The manufacturing process is the same as described in Section 2.1 apart from the liquid injection, which is done through openings in the back glass. After injecting the liquids, the openings are sealed using round nuts and PIB.

For the disassembly, firstly, the liquid is removed from the module after removing the round nut and PIB from the openings. Figure 9b shows the disassembled module obtained by cutting PIB manually from the edge and separating the front from the back glass. Following this, the solar cell and the busbars are removed. Figure 9c shows the process of scraping the PIB from the edge. The cleaned glass, along with recovered PIB, is shown in Figure 9d. Therefore, all the module components are separated, which can be either reused or recycled separately.

The glass sheets (Figure 9d) are further cleaned with isopropyl alcohol to remove any chemical residue before reusing in new modules. Silicon solar cell with busbars extracted from an air-filled module is reused to make new modules. The modules made with the reused components showed similar efficiency to the new modules. PIB is not reused because of its interaction with liquid and possible loss of its structural properties. We further aim to carry out a detailed study in future to evaluate the properties of each component after usage and explore their extent of circularity.

4 | Discussion and Outlook

In this study, one-cell module prototypes are used to investigate the potential of liquid-filled modules. Considering the positive results, we aim to scale up the module size with some design alterations in the future. Figure 9a shows the prototype of a new module design, where back glass with resealable openings is used to ease the liquid injection and removal process. Moreover, with the increased number of Si cells, glue dots will be placed on the glass sheet, as a spacer, to avoid cracks in the cells during PIB sealing. We also aim to extend our research by using other liquids and edge sealants. Along with this, further studies will be carried out to study the stability of liquid-filled modules under ultraviolet light.

Furthermore, we will investigate the stability of perovskite/c-Si tandem solar cells upon liquid encapsulation. Ideally, liquid encapsulation of the tandem cell should prevent moisture ingress in the perovskite cell, which can improve the stability of perovskite. Recent work by Mariani et al. also showed that a liquid/semi-solid encapsulant can improve stability and reduce thermo-mechanical stress in perovskite solar cells [61].

In a photovoltaic module, ~70% of irradiance is converted into thermal energy, which in turn increases the cell temperature and decreases the module's efficiency [62]. Generally, this waste thermal energy can be utilized using a coolant in a photovoltaic-thermal (PV-T) collector to deliver usable thermal energy along with efficient electrical energy [63]. In a PV-T collector, the thermal loop is separate, usually behind the PV part, thus having less direct access to the heat sources (solar cells) and requiring additional materials to manufacture. However, as our liquid encapsulated modules use cooling liquids (e.g., silicone oil), it can eventually be turned into a PV-T module without a need for additional coolant or materials to separate the loop. This can be achieved by using the encapsulated liquid in a heat loop to extract thermal energy from the module. This concept is beyond the scope of this work and will be studied separately.

5 | Conclusions

Our research is an addition to the ongoing efforts of creating circular PV modules by proposing and demonstrating a liquid encapsulation PV module for standard industrial c-Si solar cells. Four liquids (silicone oil, ester oil, glycol and glycerol) show promising results comparable to standard EVA encapsulant to be used in the liquid encapsulated PV technology. Furthermore, our optical simulation complements the experiments and strongly supports the concept of liquid encapsulation for efficient PV modules by ensuring optical matching at the glass/encapsulant interface. The new design of the liquid encapsulated module provides the following advantages: (i) easy dismantling of the photovoltaic module to individual components to recycle raw materials, (ii) comparative performance to EVA laminated PV modules and (iii) stability under various accelerated ageing conditions. Our proposed liquid encapsulation approach could be further tested in perovskite/c-Si tandem PV technology for boosting stability. In addition, liquid encapsulation could exploit heat dissipation in the PV module enabling an upgrade into a PV-T module architecture by using the liquid in a heat exchange loop. Through this study, we aim to put forward new technology for encapsulation and demonstrate that an efficient circular PV module can be achieved with ongoing research.

Author Contributions

Urvashi Bothra: experiments, analysis, writing – original draft preparation and editing. **Sebastian Weemaes:** experiments, analysis, review and editing. **Thomas Rijsman:** simulations, analysis, review. **Alberto Poli:** experiments, review. **Siemen Brinksma:** review and editing. **Olindo Isabella:** review and editing, supervision. **Malte Ruben Vogt:** supervision, review and editing.

Acknowledgements

We would like to thank Stefaan Heirman for his help in customizing experimental setups and suggesting innovative ideas. We thank Ian Lin for his help in module manufacturing and Juan Camilio Ortiz Lizcano for fruitful discussion on how to simulate the cells. We also thank Dr. Bálint Fodor from Semilab for measuring the refractive index of silicone oil, ester oil and glycerol.

Funding

We would like to acknowledge funding from Kennis en Innovatie Agenda – Circulaire Economie 2023 under FAIR-PV: Future Repairable, Transparent and Sustainable Solar-PV (KIACE-23-03580445). TU Delft's Climate Action Program Flagship project "Materials for circular renewable energy technologies" supported this work.

Conflicts of Interest

The authors declare no conflicts of interest.

Data Availability Statement

The data that support the findings of this study are available on request from the corresponding author. The data are not publicly available due to privacy or ethical restrictions.

References

1. Paris agreement, *UN Climate Change Conference* (United Nations Treaty Series, 2015).

2. O. L. d'Ortigue, A. Whiteman, and S. Elsayed, *Renewable Energy Capacity Statistics 2015* (International Renewable Energy Agency, 2015).

3. IRENA, *Renewable Capacity Statistics 2025* (International Renewable Energy Agency, 2025).

4. *Levelized Cost of Energy +*. LAZARD. p. 48.

5. IRENA, *World Energy Transitions Outlook 2022: 1.5°c Pathway* (International Renewable Energy Agency, 2022).

6. C. Xu, O. Isabella, and M. R. Vogt, ""Future Material Demand for Global Silicon-Based PV Modules Under Net-Zero Emissions Target Until 2050," *Resources*," *Conservation and Recycling* 210 (2024): 107824, https://doi.org/10.1016/j.resconrec.2024.107824.

7. G. Imbuluzqueta, F. J. Cano, U. Iglesias, et al., "Photovoltaic Module With Encapsulant System Based on Recyclable Composite Material," *Solar Energy* 300 (2025): 113799, https://doi.org/10.1016/j.solener.2025.113799.

8. K. Agroui, M. Jaunich, and A. H. Arab, "Analysis Techniques of Polymeric Encapsulant Materials for Photovoltaic Modules: Situation and Perspectives," *Energy Procedia* 93 (2016): 203–210, https://doi.org/10.1016/j.egypro.2016.07.171.

9. A. Alhodaib, Z. Yahya, O. Khan, et al., "Sustainable Coatings for Green Solar Photovoltaic Cells: Performance and Environmental Impact of Recyclable Biomass Digestate Polymers," *Scientific Reports* 14, no. 1 (2024): 11221, https://doi.org/10.1038/s41598-024-62048-5.

10. D. Mao, S. Yang, L. Ma, et al., "Overview of Life Cycle Assessment of Recycling End-of-Life Photovoltaic Panels: A Case Study of Crystalline Silicon Photovoltaic Panels," *Journal of Cleaner Production* 434 (2024): 140320, https://doi.org/10.1016/j.jclepro.2023.140320.

11. M. Rames, *Technical Support for the Development of a Recyclability Index for Photovoltaic Products* (European Climate, Infrastructure and Environment Executive Agency (CINEA), 2025).

12. K. Wambach, C. Libby, and S. Shaw, *Advances in Photovoltaic Module Recycling: Literature Review and Update to Empirical Life Cycle Inventory Data and Patent Review* (IEA PVPS TCP, 2024).

13. FLAXRES GmbH, (2025), 22/07/2025, https://www.flaxres.com/en/flaxres-a-new-era-of-photovoltaik-recycling/.

14. LuxChemtech GmbH, (2025), 22/07/2025, https://lc-freiberg.de/?lang=en.

15. "Npc Incorporated: Recycling of Solar Panels," (2025), 22/07/2025, https://www.npcgroup.net/eng/solarproduct/reuse-recycle/recycle-service.

16. G. A. Heath, T. J. Silverman, M. Kempe, et al., "Research and Development Priorities for Silicon Photovoltaic Module Recycling to Support a Circular Economy," *Nature Energy* 5, no. 7 (2020): 502–510, https://doi.org/10.1038/s41560-020-0645-2.

17. M. Calì, B. Hajji, G. Nitto, and A. Acri, "The Design Value for Recycling End-of-Life Photovoltaic Panels," *Applied Sciences* 12, no. 18 (2022): 9092, https://doi.org/10.3390/app12189092.

18. A. K. Schnatmann, F. Schoden, and E. Schwenzfeier-Hellkamp, "Sustainable PV Module Design—Review of State-of-the-Art Encapsulation Methods," *Sustainability* 14, no. 16 (2022): 9971, https://doi.org/10.3390/su14169971.

19. R. Einhaus, K. Bamberg, R. D. Franclieu, and H. Lauvray, "New Industrial Solar Cell Encapsulation (Nice) Technology for PV Module Fabrication at Drastically Reduced Costs," in *19th European Photovoltaic Solar Energy Conference*, vol. 1, (2004): 2371.

20. J. Dupuis, E. Saint-Sernin, O. Nichiporuk, P. Lefillastre, D. Bussery, and R. Einhaus, *Nice Module Technology - From the Concept to Mass Production: A 10 Years Review* (*IEEE*, 2011).

21. J. Dupuis, E. Saint-Sernin, K. Bamberg, et al., *Iec Certification and Extended Ageing Test of Nice Modules* (EUPVSEC, 2010).

22. M. Mittag, T. Neff, S. Hoffmann, M. Ebert, U. Eitner, and H. Wirth, *Tpedge: Glass-Glass Photovoltaic Module for bipv-Applications* (Engineered Transparancy, 2016).

23. D. Reinwand, B. King, J. Schube, F. Madon, R. Einhaus, and D. Kray, *Lab-Scale Manufacturing of Medium Sized N.I.C.E. Modules With High-Efficiency Bifacial Silicon Heterojunction Solar Cells* (Metallization and Interconnection for Crystalline Silicon Solar Cells, 2019).

24. M. Mittag, U. Eitner, and T. Neff, "Tpedge: Progress on Cost-Efficient and Durable Edge-Sealed PV Modules," in *33rd European PV Solar Energy Conference and Exhibition* (2017).

25. H. Li, *The Optical Property and Degradation of Liquid Encapsulated Solar Cells* (TU Delft, 2024), 1–25.

26. Y. Kroon, "Pv Solar Exploration: The Circular Photovoltaic-Thermal Panel of the Future," in *Faculty of Industrial Design Engineering* (TU Delft, 2024), 59.

27. A. Perelman, V. Barth, F. Mandorlo, and E. Voroshazi, "Innovative Design-for-Recycling for Critical Material-Free Interconnection of PV Modules," *Progress in Photovoltaics: Research and Applications* 34 (2025): 18–28, https://doi.org/10.1002/pip.3869.

28. *Solar Photovoltaic Energy Systems-Terms, Definitions and Symbols* (International Electrotechnical Commission, 2016): 1–13.

29. IEC, "Iec-61215-1:Terrestrial Photovoltaic (pv) Modules - Design Qualification and Type Approval Part 1: Test Requirements," in *Internation Standard* (2021).

30. R. Santbergen, T. Meguro, T. Suezaki, G. Koizumi, K. Yamamoto, and M. Zeman, "Genpro4 Optical Model for Solar Cell Simulation and Its Application to Multijunction Solar Cells," *IEEE Journal of Photovoltaics* 7, no. 3 (2017): 919–926.

31. T. Rijsman, *Spectral Characterisation and Optical Simulation of Innovative Liquid Encapsulants for Design-for-Recycling Silicon Solar Modules, in EEMCS* (TU Delft, 2025).

32. J. C. O. Lizcano, P. Procel, A. Calcabrini, et al., "Colored Optic Filters on c-Si IBC Solar Cells for Building Integrated Photovoltaic Applications," *Progress in Photovoltaics: Research and Applications* 30, no. 4 (2021): 401–435, https://doi.org/10.1002/pip.3504.

33. C. Peike, I. Hädrich, K.-A. Weiß, and I. Dürr, *Overview of PV Module Encapsulation Materials* (*Fraunhofer IS*, 2013), https://www.pv-tech.org.

34. *Technical Data Sheet of Xiameter pmx-561 Transformer Liquid* (DOW Chemical Company, 2019).

35. *Technical Brochure of mivolt dfk Immersion Cooling Liquid* (MIDEL & MIVOLT Fluids Ltd, 2024).

36. *Technical Datasheet of Electrocool Dielectric Coolants* (Engineering Fluids, 2023).

37. D. Childs, *Technical Manual of Opticool Fluids* (DSI Ventures, 2014).

38. *Technical Datasheet of Innogreen Solarpro*. InnogreenChem.

39. *Technical Datasheet of Monopropyleneglycol* (Labshop, 2019).

40. *Datasheet MPG-Industrial PO & Derivatives* (Shell Chemicals, 2019).

41. *Technical Datasheet of Glycerine 99.5%* (Netherlands, 2024).

42. J. D. Hepburn, F. E. Vermeulen, and F. S. Chute, "Resistivity of Nai-Glycerol Solutions," *AIAA* 9 11 (2012): 2270–2271, https://doi.org/10.2514/3.6498.

43. *Application Bulletin Deionized Water* (M.L. COMPANY, 2021).

44. M. Daimon and A. Masumura, "Measurement of the Refractive Index of Distilled Water From the Near-Infrared Region to the Ultraviolet Region," *Applied Optics* 46 (2007): 3811–3820.

45. R. J. Crawford and J. L. Throne, *Rotational Molding Technology* (ScienceDirect, 2002).

46. V. Fiandra, L. Sannino, C. Andreozzi, G. Flaminio, and M. Pellegrino, "New PV Encapsulants: Assessment of Change in Optical and Thermal Properties and Chemical Degradation After UV Aging," *Polymer Degradation and Stability* 220 (2024): 110643, https://doi.org/10.1016/j.polymdegradstab.2023.110643.

47. W.R.P.M.C. Ltd, *High-Volume Resistivity EVA (Ethylene Vinyl-Acetate Copolymer) Rubber Film and Preparation Process Thereof* (Zhejiang Lichang Technology Co., Ltd, 2013).

48. M. R. Vogt, H. Holst, H. Schulte-Huxel, et al., "Optical Constants of UV Transparent EVA and the Impact on the PV Module Output Power Under Realistic Irradiation," *Energy Procedia* 92 (2016): 523–530, https://doi.org/10.1016/j.egypro.2016.07.136.

49. HUCHEM. *Demi water*. 20/08/2025, https://www.huchem.nl/demi-water.html.

50. B. Analytiq. *Ethylene Vinyl Acetate (EVA) Price Index*. 20/08/2025, https://businessanalytiq.com/procurementanalytics/index/ethylene-vinyl-acetate-eva-price-index/.

51. ZAUBA. *Pmx 561 Imports Under hs Code 39100020*. 20/08/2025, https://www.zauba.com/import-pmx-561/hs-code-39100020-hs-code.html.

52. Y. Shao, S. Yan, J. Li, et al., "Stretchable Encapsulation Materials With High Dynamic Water Resistivity and Tissue-Matching Elasticity," *ACS Applied Materials & Interfaces* 14, no. 16 (2022): 18935–18943, https://doi.org/10.1021/acsami.2c03110.

53. SUNPOWER, *Maxeon gen 3 Datasheet*.

54. H. Hanifi, C. Pfau, D. Dassler, et al., *Investigation of Cell-to-Module (Ctm) Ratios of PV Modules by Analysis of Loss* (Fraunhofer Center for Silicon Photovoltaics, 2016), http://www.pv-tech.org.

55. Y. A. Abrahamyan, V. I. Serago, V. M. Aroutiounian, et al., "The Efficiency of Solar Cells Immersedin Liquiddielectrics," *Solar Energy Materials and Solar Cells* 73 (2002): 367–375.

56. Y. A. Abramyan, G. G. Karamyan, and A. A. Murodyan, "Effect of Liquid Dielectrics on the Efficiency of Silicon Solar Cells," *Semiconductors* 33, no. 12 (1999): 1320–1321, https://doi.org/10.1134/1.1187917.

57. X. Han, Y. Wang, and L. Zhu, "Electrical and Thermal Performance of Silicon Concentrator Solar Cells Immersed in Dielectric Liquids," *Applied Energy* 88, no. 12 (2011): 4481–4489, https://doi.org/10.1016/j.apenergy.2011.05.037.

58. Sinovoltaics. *Iec 61215 certification testing*. 22/07/2025, https://sinovoltaics.com/iec-61215-certification-testing/.

59. M. Owen-Bellini, P. Hacke, D. C. Miller, et al., "Advancing Reliability Assessments of Photovoltaic Modules and Materials Using Combined-Accelerated Stress Testing," *Progress in Photovoltaics: Research and Applications* 29, no. 1 (2020): 64–82, https://doi.org/10.1002/pip.3342.

60. S. Kurtz, K. Whitfield, D. Miller, et al., "Evaluation of High-Temperature Exposure of Rack-Mounted Photovoltaic Modules," in *2009 34th IEEE Photovoltaic Specialists Conference (PVSC)* (IEEE, 2009), 2399–2404.

61. P. Mariani, M. A. Molina-Garcia, J. Barichello, et al., "Low-Temperature Strain-Free Encapsulation for Perovskite Solar Cells and Modules Passing Multifaceted Accelerated Ageing Tests," *Nature Communications* 15, no. 1 (2024): 4552, https://doi.org/10.1038/s41467-024-48877-y.

62. Z. Ul-Abdin, M. Zeman, O. Isabella, and R. Santbergen, "Investigating the Annual Performance of Air-Based Collectors and Novel Bi-Fluid Based PV-Thermal System," *Solar Energy* 276 (2024): 112687, https://doi.org/10.1016/j.solener.2024.112687.

63. R. M. Elavarasan, V. Mudgal, L. Selvamanohar, et al., "Pathways Toward High-Efficiency Solar Photovoltaic Thermal Management for Electrical, Thermal and Combined Generation Applications: A Critical Review," *Energy Conversion and Management* 255, no. 115278 (2022): 1–31, https://doi.org/10.1016/j.enconman.2022.115278.

Supporting Information

Additional supporting information can be found online in the Supporting Information section. **Table S1:** Lamination conditions for manufacturing air-filled, liquid-filled, and EVA encapsulated modules. **Table S2:** Thermal conductivity of the selected liquids used in this work. **Table S3:** Average transmittance from 400 to 1100 nm of the encapsulants (air, liquids and EVA) laminated between the glasses. **Table S4:** Comparison of measured short circuit current density (J_{SC}) by *J-V* scan and simulated J_{SC} of the device stack for different encapsulants. **Table S5:** Overview of all experiments performed with different encapsulants in this work. ✓ represents encapsulant that passed the test and x represents failure of encapsulant, along with the reason. After failing, the boxes are highlighted red for subsequent tests of an encapsulant. Encapsulants, which performed similarly, are grouped together. **Table S6:** Device performance parameters before and after glycol filling in a four-cell module (same module as in Figure 8a). **Figure S1:** Polyisobutylene (PIB edge sealant) and liquid interactions. (a) Images of glass/liquid/glass sandwich structures with silicone oil, hydrocarbon-E, ester oil and hydrocarbon-O liquids. (b) Images of the prototype after keeping them in ambient for 4 months. Hydrocarbon-O interacted with the sealant and was thus removed from further studies. (c) Images of the prototypes after 300 h of damp heat test. Hydrocarbon-E interacted with the sealant and thus, removed from the study. Two more prototypes with glycol and glycerol were added. (d) Images of prototypes with silicone oil, ester, glycol and glycerol after 51 thermal cycles showing no signs of interactions with PIB edge sealant. **Figure S2:** Short circuit current density, open circuit voltage and fill factor of the EVA encapsulated, air- and liquid-filled modules as a function of humidity freeze cycles.